NUMERICAL SIMULATIONS OF BOUNDARY LAYER BYPASS TRANSITION WITH LEADING EDGE EFFECTS

Victor Ovchinnikov and Ugo Piomelli
Department of Mechanical Engineering,
University of Maryland
College Park, Maryland 20742, USA
taly@eng.umd.edu, ugo@eng.umd.edu

Meelan M. Choudhari
NASA Langley Research Center
Hampton, Virginia 23681, USA
m.m.choudhari@larc.nasa.gov

ABSTRACT

This study investigates the accuracy of synthetic-turbulence inflow conditions to numerical simulations of boundary-layer bypass transition. To this end we have performed three direct numerical simulations (DNS) of boundary layer bypass transition. In two of the simulations the inflow condition is imposed downstream of the leading edge and the free-stream turbulence is attenuated inside the boundary layer using two prescribed *ad hoc* attenuation profiles. In the third simulation we included the leading edge of the flat plate inside the computational domain; thus we were able to follow the physical evolution of free-stream turbulence above the flat plate. The results of the latter simulation reveal the presence of small-amplitude laminar streaks at the streamwise location corresponding to the inflow boundary of the truncated-domain simulations. Because the b.l. streaks are not modeled by the inflow specification for the truncated-domain simulations, such simulations may not be expected to provide reliable predictions of the bypass transition process. However, our simulations underline qualitative similarities between the flow fields in all three cases. Thus it is possible that, with suitable calibration, truncated-domain simulations may be a useful tool for investigating the physical mechanisms of bypass transition.

INTRODUCTION

Transition prediction has its place among the most important practical problems in fluid dynamics today. Among its applications are optimization of low-pressure turbine and airfoil design, in which it is frequently desirable to delay transition to turbulence or avoid boundary layer separation. For this reason, the recent years have witnessed extensive experimental, theoretical, and numerical work on boundary layer receptivity and turbulent transition. In a realistic disturbance environment such as the one over a typical airfoil, transition is described by the "bypass" mechanism, a term referring primarily to the absence of the classical TS waves in the transition process. Although the phenomenon of bypass transition has been well-studied through experiments, more insightful numerical simulations have been made difficult by the formidable cost of computation, even at low Reynolds numbers (see Rai & Moin, 1993, Voke & Yang, 1994, Jacobs & Durbin, 2001). With the possible exception of Rai & Moin (1993), the above studies did not account for the flat plate leading edge region.

We have recently carried out several bypass transition simulations (Ovchinnikov *et al.* 2004) with the aim of investigating the effects of various inflow parameters on the onset of transition. In particular, we observed that boundary layer bypass transition is strongly dependent on the integral length scale of the free-stream noise and the extent of its penetration into the boundary layer. By varying within a sensible range the simulation parameters that were not specified in the reference experiment (Roach & Brierlay, 1992) we were able to move the transition onset upstream or downstream at a fixed level of free-stream turbulence. These results indicated that, in order to specify the problem fully (1) a reliable value for the length scale of the free-stream turbulence, and (2) the extent of disturbance penetration into the boundary layer must be available from experiments. Simulations may also need to match experimental Reynolds-stress profiles inside the boundary layer well upstream of the transition location.

Alternatively, in order to avoid the problem of specifying the near-wall behavior altogether, numerical simulations could include the boundary-layer leading edge. To investigate the difference between simulations with an artificial disturbance profile and those that include the leading-edge, we present a simulation with a super-elliptical leading-edge that is represented using the immersed boundary method (implemented according to Balaras, 2004). The super-ellipse is only a convenient choice of leading-edge modeling that avoids velocity discontinuities in a simulation; the effect of leading-edge geometry may be another significant factor and is not investigated here. The simulation is performed on a Cartesian coordinate system inside a multi-block domain. Through a simulation of this type it is possible to follow the development of the free-stream disturbance near the boundary layer edge, and monitor the extent of its penetration into the boundary layer. Furthermore, it should be possible to make more general conclusions about the universal applicability of the inflow-condition methods proposed in the past, and on the effect of *ad hoc* parameters in these methods. Our primary emphasis at this stage is on using statistical fluid metrics to gauge the effect of various inflow treatments. Detailed investigation of transition physics

is deferred to a later stage.

PROBLEM FORMULATION

In this work we use the incompressible Navier-Stokes equations to perform DNS simulations of boundary layer transition under free-stream turbulence. The equations of motion

$$\frac{\partial u_j}{\partial x_j} = 0, \tag{1}$$

$$\frac{\partial u_i}{\partial t} + \frac{\partial}{\partial x_j}(u_j u_i) = -\frac{1}{\rho}\frac{\partial p}{\partial x_i} + \nu \nabla^2 u_i, \tag{2}$$

are solved numerically using a second-order accurate finite-difference method on a staggered grid. The method fully conserves mass, momentum and kinetic energy in the discrete sense (see Morinishi *et al.*, 1998). The coordinates x, y and z refer, respectively, to the streamwise, spanwise and wall-normal directions. The velocity components in these directions are, respectively, u, v and w. All grids used are uniform in the spanwise direction y, stretched in the streamwise and wall-normal directions to allow accurate resolution of boundary layer disturbances, particularly in the transitional region. The discretized equations are integrated in time using an explicit fractional time-step method, (Chorin, 1968, Kim & Moin, 1985) in which all terms are advanced in time using the Adams-Bashforth method. The Poisson equation is solved, and the velocity is corrected to make the field solenoidal. The code has been extensively validated for a variety of turbulent (Balaras *et al.*, 1995, Balaras *et al.*, 2001) and re-laminarizing (Piomelli *et al.*, 2000) flows.

The code was parallelized with the MPI message-passing protocol. The computational box is divided into n subdomains in the streamwise direction, and each of the n processors integrates the equations of motion in one of the subdomains. The pressure field is obtained by applying spanwise FFT to the Poisson equation. This yields a pentadiagonal matrix for each Fourier mode, which is then inverted by a cyclic reduction algorithm. Each processor is assigned a subset of the Fourier modes resulting from the application of FFT.

Initial and boundary conditions

Two types of simulations of boundary layer transition have been carried out. In the first type (truncated-domain), the inflow plane is located downstream of the flat-plate leading edge. In this case our computational domain is a rectangular box with dimensions $L_x \times L_y \times L_z = 620\delta^o_{98} \times 30\delta^o_{98} \times 40\delta^o_{98}$, where δ^o_{98} is the 98% thickness of the laminar boundary layer at the inlet[1]. The inlet is located at $Re_\theta \simeq 50$, ($Re_x = 5,520$, $x = 15$). At the outflow, δ_{98} is approximately 1/4 of the wall-normal domain.

In the second type (full-domain) we used the same length scale as in the first type (*i.e.* δ^o_{98}) and our computational domain consisted of two boxes with dimensions $L_x \times L_y \times L_z = 50\delta^o_{98} \times 30\delta^o_{98} \times 40\delta^o_{98}$ and $L_x \times L_y \times L_z = 720\delta^o_{98} \times 30\delta^o_{98} \times 38.7\delta^o_{98}$, respectively. The multi-block approach is necessary because, in order to resolve properly the formation of the boundary layer around the leading edge, very fine wall-normal grid resolution is required that is not necessary throughout the entire domain. In the first box we used the immersed boundary method to represent a flat plate with a super-elliptical leading edge (see Lin *et al.*, 1992) with radius 1.3 and aspect ratio 6. In order to validate the immersed-boundary representation of the leading-edge, we simulated laminar flow around a superellipse of aspect ratio 6, at $Re = 2,400$, based on the plate half-thickness, and obtained excellent agreement with data of Lin *et al.* (1992). To avoid excessive computational cost, only the top half of the super-ellipse was modeled, and a symmetry condition was used on the bottom boundary. The symmetry condition is not physical, since it anchors the flow stagnation point to the tip of the super-ellipse. We do not expect this to be a significant source of error, however, since the fluctuations in the stagnation point location should be small. Nevertheless, their effect on transition characteristics needs to be ascertained. A more costly simulation without the symmetry condition is currently underway. The flow configuration is sketched in Figure 1. The inflow boundary is located at $x = -20$, inside the first box, the leading edge being at $x = 0$. At location $x = 20$, corresponding to $Re_x = 7,280$, cross-stream velocity planes were saved and used as the inflow condition for the second box. At the outflow of the second box δ_{98} was approximately 1/3 of the wall-normal domain. All streamwise distances quoted in this article are measured relative to the leading edge.

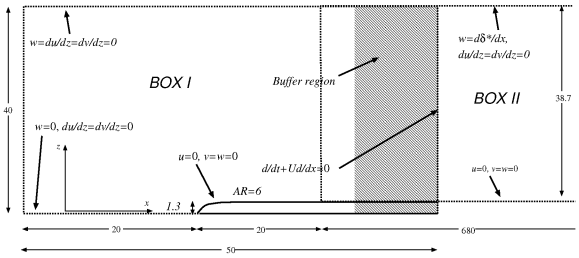

Figure 1: Schematic of the geometry for the full-domain simulation

The following boundary conditions were applied:

1. In the truncated-domain simulations, the inlet velocities are imposed by adding zero-mean perturbations to the Blasius base-flow. The disturbance was generated using the modified Rogallo (1981) algorithm as implemented by Jacobs and Durbin (2001) with Fourier modes (see Ovchinnikov et al., 2004, for details). The disturbance field was multiplied by an attenuation profile f, which was smoothly decreased from $f = 1$ in the free stream to $f = 0$ at the plat surface to mimic the shear-sheltering of the boundary layer (see Jacobs & Durbin, 1998), which hampers the penetration of turbulence towards the wall. The attenuation profiles, plotted in Figure 3, are defined as

$$f = 1 - \frac{tanh\left(7\left(z_0 - z\right) + 1\right)}{tanh\left(7\right) + 1}, \tag{3}$$

where z_0 is the inflection point location of the attenuation profile. For Truncated I and II cases, $z_0 = 1.0$ and 1.5, respectively.

Similarly, the inflow for the first box of the full-domain simulation was obtained by adding a zero-mean field to a uniform mean velocity profile. The inflow condition for the second box was obtained by interpolating

[1] Taking the location of 98% of the velocity maximum removed small-amplitude fluctuations of the velocity around its free-stream mean. The ratio δ_{98}/δ_{99} was about 0.9

velocities from the first box onto the wall-normal grid of the second box as mentioned above. In all cases, the initial free-stream turbulence (f.s.t.) integral length scale was $3.0\delta^o_{98}$ and the target f.s.t. intensity was 6% at $(x = 15, Re_x = 5,520)$ In all simulations, downstream of a short transient, the f.s.t. intensity decayed as a power law $(x - x_0)^{-\alpha}$ with $\alpha \approx 0.7$

2. At the outlet convective boundary conditions (Orlanski, 1976) were applied. Simulation results in the last 10% of the domain were discarded due the proximity of the outflow boundary condition.

3. In the spanwise direction, y, periodic conditions were used.

4. At the free-stream boundary of the truncated-domain simulations and the second box of the full-domain simulation, we imposed $u = 1$, $v = 0$, $w = d\delta^*/dx$, where δ^* is computed for the Blasius profile. In these simulations the acceleration coefficient $\mathrm{K} \equiv -(\nu/U^2_\infty)(dU_\infty/dx)$ was of the order of 10^{-7}. The value of K at which a turbulent boundary layer is expected to re-laminarize is around 3.0×10^{-6} (Spalart, 1986). Since in our case K is an order of magnitude lower, we do not expect the acceleration to affect transition significantly. For the first box of the Full-domain simulation we used a slip-wall boundary condition on the free-stream boundary. The resulting acceleration of the free-stream was mild, with $K \simeq 10^{-7}$.

5. No-slip conditions were used on the bottom wall of the truncated-domain simulations, the bottom wall of the second box of the full-domain simulation, and the leading edge of the first box.

RESULTS

The grid requirements for DNS of boundary-layer bypass transition can be found in various sources (Rai & Moin, 1993, Jacobs & Durbin, 2001, Ovchinnikov *et al.*, 2004). As a general rule, the streamwise and spanwise grid spacing should be under $\Delta x^+ = 12$, $\Delta y^+ = 6$ with the same wall-normal resolution as needed for DNS of the turbulent boundary layer. Simulation parameters are summarized in Table 1 and the streamwise mesh spacing is shown in Fig. 2, which also shows the streamwise resolution used by Jacobs & Durbin (2001), who also used a code similar to ours.

The initial purpose of the truncated-domain simulations was to capture the region of transition onset accurately (as judged by the skin friction rise and the turbulent kinetic energy budgets), but not its final stages, or the fully-turbulent regime. While this significantly reduces computational cost, it limits the region of reliable data to the maximum of $x = 275, Re_x = 100,100$ (see Figure 2). Consequently, in all of the plots that follow, data from truncated simulations has been restricted to this region. Data from the full-domain simulation, in contrast, are reliable up to $x \simeq 660, Re_x \simeq 240,000$.

In the figures that show streamwise evolution of various quantities, we plot a dotted vertical line at location $x = 220$, $Re_x = 80,080$ to denote the middle of skin friction rise. The skin friction coefficient, which shows a characteristic rise in transition, is defined as

$$C_f = \frac{\tau_w}{\frac{1}{2}\rho U^2_\infty}. \quad (4)$$

Table 1: Summary of simulation parameters.

Case	$nx \times ny \times nz$	Δx^+	Δy^+	Δz^+_{min}
Truncated I	$900 \times 180 \times 150$	Fig.2	3.0	1.0
Truncated II	$900 \times 180 \times 150$	Fig.2	2.5	0.5
Full Box I	$288 \times 192 \times 222$	Fig.2	2.4	0.5
Full Box II	$1474 \times 192 \times 159$	Fig.2	2.5	0.8

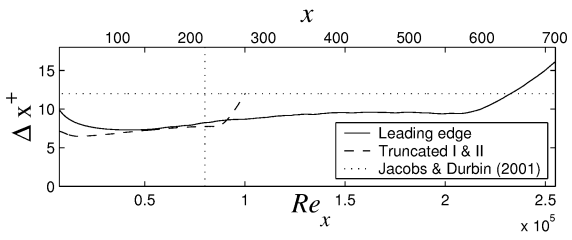

Figure 2: Streamwise mesh spacing in wall units

The difference between Truncated I and Truncated II cases is the choice of the attenuation profile, shown in Figure 3. As can be seen, in case I, turbulence is placed closer to the wall than in case II, in which the disturbance profile attenuates rapidly just inside the boundary-layer edge.

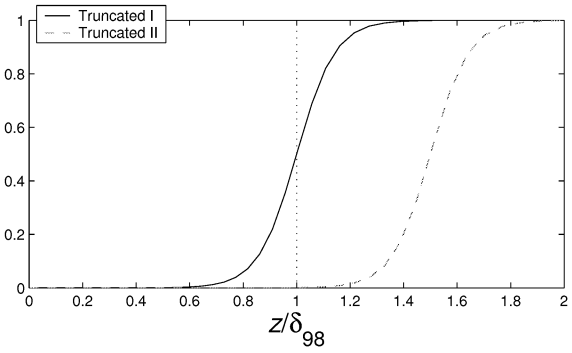

Figure 3: Attenuation ptofiles used in truncated-domain simulations

In order to permit a direct comparison between the three simulations, the external disturbance environment must be the same. This means that the type of disturbance, its integral length scale and intensity should be identical. Since in the full-domain simulation our inflow plane was located $40\delta^o_{98}$ upstream of the truncated-domain inflow plane, we were required to experiment with the intial disturbance amplitude and length scale of the Full-domain inflow in order to match the initial amplitude (6%) and decay rate of the truncated-domain simulations. The f.s.t. intensities are shown in Figure 4. It can be seen that the f.s.t. level in the full-domain simulation is slightly above the target value. This discrepancy,

however, is small and should not be sufficient to cause a major shift in the onset of transition.

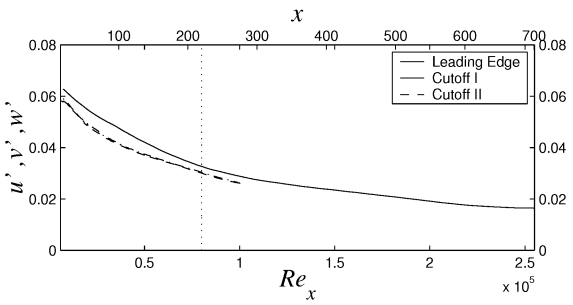

Figure 4: Evolution of f.s.t. intensity

In addition, because the full-domain simulation inflow is located upstream of the truncated-domain simulation inflow, the boundary layer in the former (due to the f.s.t. and the leading edge geometry) could potentially evolve differently and result in a different mean flow, which would complicate comparisons with the truncated simulations. To investigate this possibility, in Figure 5 we show the streamise evolution of the displacement and momentum thicknesses for the three simulations, which are defined as

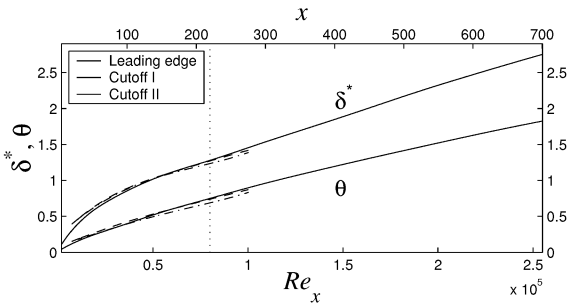

Figure 5: Streamwise evolution of displacement and momentum thickness

$$\delta^* = \int_0^{y_{max}} \left(1 - \frac{\langle U \rangle}{U_\infty}\right) dy, \tag{5}$$

$$\theta = \int_0^{y_{max}} \frac{\langle U \rangle}{U_\infty} \left(1 - \frac{\langle U \rangle}{U_\infty}\right) dy. \tag{6}$$

The good agreement in these quantities indicates that the mean flows preceding the onset of transition are very similar for the three cases.

As stated before, in truncated simulations an attenuation profile is used to bring the turbulence to zero at the flat plate. With the exception of the work of Jacobs and Durbin (2001), this profile is entirely arbitrary, *i.e.*, no generally accepted theory on the depth and shape of the penetration profile exists. To shed some light on this matter, in Figure 6 we show profiles of the turbulent kinetic energy (TKE), defined as $k = \langle u_i' u_i' \rangle / 2$ (a prime denoting a fluctuation), inside the boundary layer at locations $x = 25$; 75; 175; 275, ($Re_x = 27,300$; 63,700; 100,100; 182,000) for the three simulations (see Figure 3 for attenuation profiles). The first location is fully within the perturbed laminar boundary layer, the second is at the location of transition onset (judging by the skin friction rise) and the last, near the end of transition. The wall-normal coordinate is normalized with the Blasius similarity variable $\eta = \sqrt{\nu U_\infty / x}$. The laminar boundary layer edge corresponds to $z/\eta \simeq 4.9$. At location $x = 25$ the full-domain simulation shows nearly the same kinetic energy as the Truncated II case. The maximum TKE corresponding to the Truncated I case is twice that of the full-domain case. However, from that location on, the growth of the TKE inside the boundary layer for the full-domain case surpasses that of the other cases, so that by location $x = 75$ the maximum boundary layer TKE for the full case is 20% larger than that of the Truncated I case. By location $x = 275$, which is at the beginning of the fully-turbulent region, all three cases show very similar TKE levels, suggesting that a turbulent equilibrium is being established. For more detail, in Figure 7 we show the streamwise evolution of the maximum Reynolds stresses inside the boundary layer (normalized by the friction velocity, u_τ, defined as $\sqrt{\tau_w/\rho}$). One can see the prominent growth of $\langle uu \rangle$, larger in the full domain case than in the others, which is followed by a decay towards a turbulent equilibrium in all three cases. The growth, linear-like in the region $x = 25 - 75$, is present only in the streamwise component of the Reynolds stress, which is magnified in Figure 8 and normalized by U_∞. From this plot one can also see that the truncated-domain simulations show an initial transient in which the streamwise stress is oscillatory. This may indicate that in the truncated simulations the inflow disturbance lacks the proper phase information inside the boundary layer and produces a lower disturbance growth-rate. The result is an early transitional stage in which the Reynolds stresses do not match the values of the full-domain simulation.

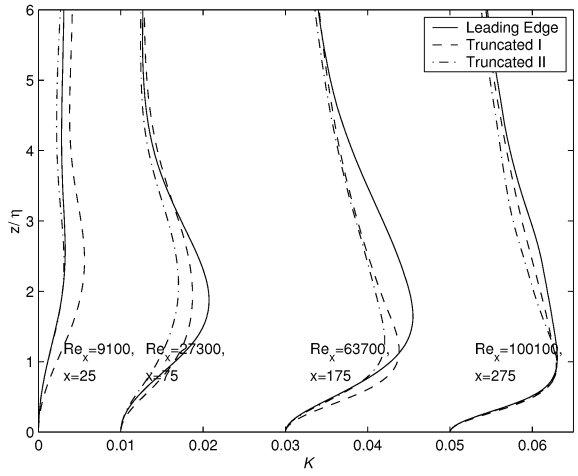

Figure 6: Profiles of turbulent kinetic energy vs. z/η

It has been shown experimentally and numerically (see, for example, Matsubara & Alfredsson, 2001, and Jacobs & Durbin, 2001) that boundary-layer interaction with moderate-amplitude f.s.t. is characterized by the appearance of low-frequency streaks of streamwise velocity[2] inside the perturbed laminar and early transitional boundary layer. Transition is postulated to occur via streak instability and breakdown.

Examination of the flow field in our simulations revealed the presence of near-wall streaks in all three cases. Figure 9 shows the contours of the streamwise velocity fluctuation in

[2]Also known as Klebanoff (1971) modes

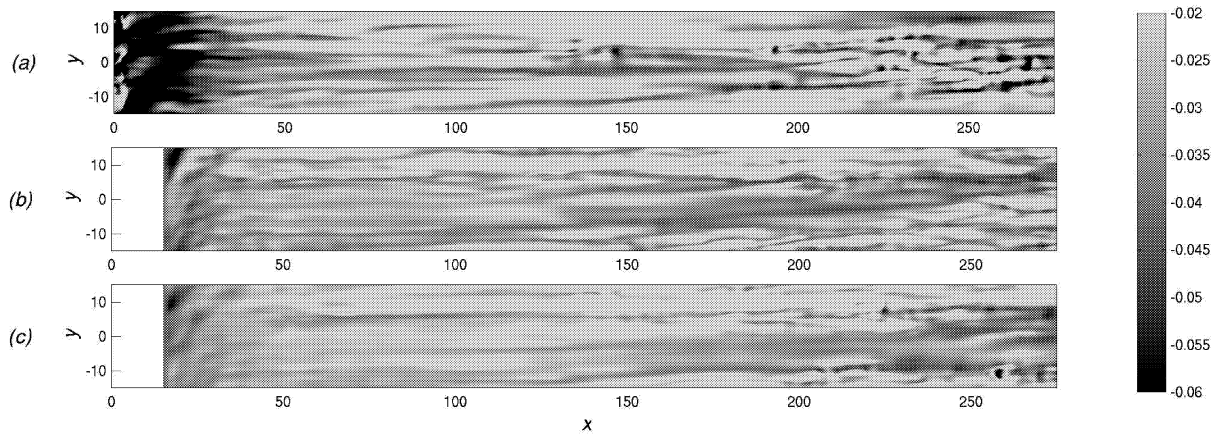

Figure 9: Contours of streamwise velocity fluctuation at $z = 0.05$; (a) Full-domain, (b) Truncated I (c) Truncated II

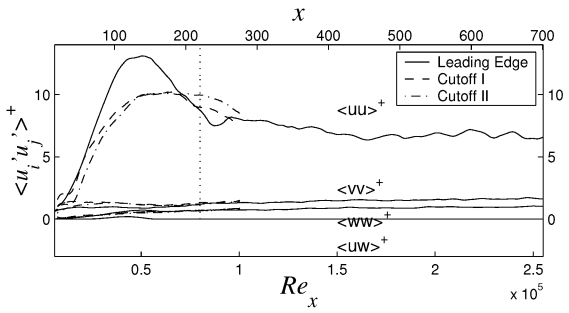

Figure 7: Streamwise evolution of maximum Reynolds stress levels inside the boundary layer normalized by the friction velocity

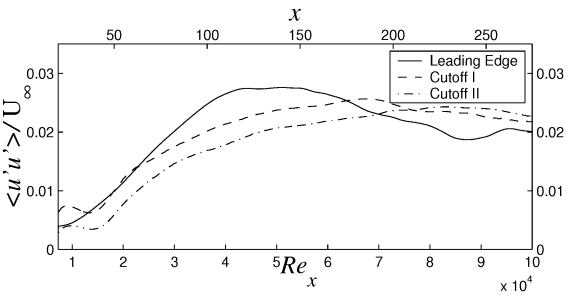

Figure 8: Streamwise evolution of maximum $\langle u'u' \rangle$ stress levels inside the boundary layer normalized by the free-stream velocity

a plane parallel to the wall at $z = 0.05$, which at location $x = 15$, $Re_x = 5,500$ corresponds to 5% of the boundary layer thickness δ_{98}. The qualitative similarity of the plots away from the inlet suggests that the transition mechanism is the same in all cases. From location $x = 15$ (where the inlet into the truncated-domain simulations is located) to $x \approx 22$, however, only the full-domain plot shows incipient streaks. These streaks could also be inferred from spanwise correlation functions of the streamwise and wall-normal velocity fluctuation at $x = 15$ (not shown) At $z = 0.05$ the correlation functions are consistent with a weak structure with a spanwise separation of $\simeq 2.5\delta_{98}$.

At location $x = 100$, $Re_x = 36,400$ we observed oscillatory behavior in the correlation curves throughout the spanwise domain, consistent with strongly-correlated laminar streaks a distance 4.3 or $\simeq 1.4\delta_{98}$ apart (at this location $\delta_{98} \simeq 3.0$). Further investigation will determine whether these structures are true Klebanoff modes.

The obvious reason for the initial absence of streaks from the truncated-domain simulations is that the inlet disturbance is synthetic with random phases. Distance is required for the boundary layer to generate a physical disturbance field.

Examining the TKE budgets for the three cases revealed the importance of production, convection and pressure transport in this process. These terms are defined, respectively, as

$$-\frac{\partial \langle U_i \rangle}{\partial x_j} \langle u_i' u_j' \rangle, \qquad -\langle U_i \rangle \frac{\partial k}{\partial x_j}, \qquad -\frac{1}{\rho} \frac{\partial \langle p' u_i' \rangle}{\partial x_i}. \quad (7)$$

The convection and pressure transport terms are most active at the inflection point of the attenuation profile. By location $x \simeq 30$ the convection and pressure are much smaller than the production term and by $x = 50$ the budgets for the two cases are very similar (not shown).

In view of the discrepancies between the full- and truncated-domain simulations discussed above, it is surprising to see good agreement in the skin friction between the Truncated II case and the full-domain case that is observed in Figure 10. The fact that we were not able to match the f.s.t levels in the two simulations perfectly (cf. Figure 4) further suggests that the agreement is coincidental. Moreover, there is no *a priori* reason to choose one attennuation profile and not the other, since neither extends into the region of significant mean shear of the boundary layer, and Figure 10 shows that the onset of transition is sensitive to the choice of attenuation profile. In addition, in our simulations the inlet into the truncated-domains was arbitrarily placed at at $x = 15$. It is conceivable that shifting this location could significantly change the evolution of the streamwise streaks which, in turn, would shift the transition onset.

CONCLUSIONS

In the present study we compared DNS of boundary layer bypass transition performed in a truncated domain with a

simulation that includes the flat plate leading edge modeled as a super-ellipse. The results of the full-domain simulation indicate that at the streamwise location corresponding to the inflow boundary of the truncated-domain simulations the boundary layer already contains streaks of streamwise velocity. We also noted a higher linear-like growth of $\langle u'u' \rangle$ inside the boundary layer in the full-domain simulations in the region $x \simeq 25 - 75$, which results in an overshoot of the turbulent levels. The presence of streaks implies that the current inflow condition for the truncated-domain simulations is unphysical, since the streaks appear to be an essential feature of transition. This suggests that for accurate prediction of transition onset truncated simulations of the type presented in this study are inadequate because they cannot ensure the correct evolution of streamwse streaks. An alternative approach to inflow specification for the truncated-domain simulations would be to use a theoretical model that acccounts for the interaction of free-stream disturbance with the wall and the upstream evolution of the disturbance signature inside the boundary layer (Choudhari, 1996, Leib *et al.*, 1999). Predictions from such models were shown to provide encouraging agreement with the measured boundary-layer data for lower levels of f.s.t. (Leib *et al.* 1999). Future investigations will show whether this approach, with proper calibration, can provide accurate simulations of bypass transition.

Finally, because in the three simulations presented in this study the flow fields are qualitatively very similar, if one's aim is to study the essential physics of transition, rather than obtain an accurate quantitative prediction, truncated-domain simulations seem to be justified and cost-effective.

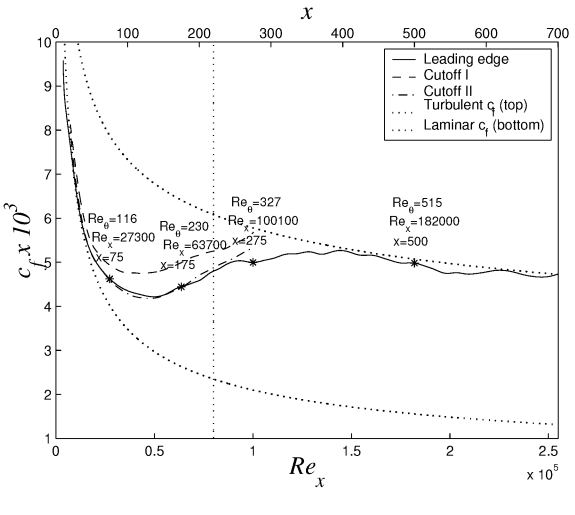

Figure 10: Streamwise evolution of the skin friction coefficient

REFERENCES

Andersson, P., Berggren, M. & Henningson, D.S., 1999 Optimal disturbances and bypass transition in boundary layers *Phys. Fluids* 11 134–150

Balaras, E., 2004 Modeling complex boundaries using an external force field on Cartesian grids in large-eddy simulations *Comput. Fluids* 33, 375–404

Balaras, E., Benocci, C., & Piomelli, U., 1995 Finite difference computations of high Reynolds number flows using the dynamic subgrid-scale model. *Theoret. Comput. Fluid Dyn.* 7, 207–216.

Balaras, E., Piomelli, U., & Wallace, J.M., 2001 Self-similar states in turbulent mixing layers *J. Fluid Mech.*, 446, 1–24.

Brandt, L., Schlatter, P., & Henningson, D. S., 2004 Transition in boundary layers subject to free-stream turbulence. *J. Fluid Mech.* 517, pp. 167–198.

Chorin, A.J., 1968 Numerical solution of the Navier-Stokes equations. *Math. Comput.* 22, 745–.

Choudhari, M. 1996 Boundary-Layer Receptivity to Three-Dimensional Unsteady Vortical Disturbances in Free Stream *AIAA Paper* 1996-0181

Fadlun, E.A., Verzicco, R., Orlandi, P., & Mohd-Yusof, J., 2000 Combined Immersed-Boundary Finite-DIfference Methods for Three- Dimensional Complex Flow SImulations *J. Comput. Phys.* 161 35–60.

Jacobs, G. J. & Durbin, P.A., 1998 Shear sheltering and the continuous spectrum of the Orr-Sommerfeld equation *Phys. Fluids* 10 2006–2011

Jacobs, G. J. & Durbin, P.A., 2001 Simulations of bypass transition *J. Fluid Mech.* 428 185–212.

Kim, J. & Moin, P., 1985 Application of a fractional step method to incompressible Navier-Stokes equations. *J. Comput. Phys.* 59 308–323.

Klebanoff, P.S., 1971 Effects of free-stream turbulence on a laminar boundary layer *Bull. Am. Phys. Soc.* 16

Leib, S. J., Wundrow, D. W., & Goldstein, M.E. 1999 Effect of free-stream turbulence and other vortical disturbances on a laminar boundary layer *J. Fluid. Mech.* 380 169–203

Lin, N., Reed, H. L., Saric, W.C., 1992 Effect of leading-edge geometry on boundary layer receptivity to free-stream sound. In "Instability, receptivity, and Turbulence", Hussaini, M., Kumar, A., Streett, C., eds. Springer-Verlag

Matsubara, M. & Alfredsson, H., 2001 Disturbance growth in boundary layers subjected to free-stream turbulence *J. Fluid. Mech.* 430 149–168

Morinishi, Y., Lund, T. S., Vasilyev, O. V., & Moin, P., 1998 Fully-conservative higher order finite difference schemes for incompressible flow *J. Comput. Phys.* 143, 90–124.

Orlanski, I., 1976 Simple boundary condition for unbounded hyperbolic flows. *J. Comput. Phys.* 21, 251–269.

Ovchinnikov, V., Piomelli, U., & Choudhari, M.M., 2004 Inflow Conditions for Numerical Simulations of Bypass Transition *AIAA Paper*, 2004-0591

Piomelli, U., Balaras, E., & Pascarelli, A., 2000 Turbulent structures in accelerating boundary layers. *J. Turbulence* 1, (001) 1–16.

Rai, M. M. & Moin, P., 1993 Direct Numerical Simulation of Transition and Turbulence in a Spatially Evolving Boundary Layer *J. Comput. Phys.* 109 169–192.

Ricco, P. and Wu, X., 2004 Effect of free-stream turbulence on a compressible laminar boundary layer, *Proc. IUTAM Symp. on Laminar-Turbulent Transition, Bangalore, Dec 13-17, 2004.*

Roach, P.E. & Brierley, D.H., 1992 In "Numerical Simulation of unsteady flows and transition to turbulence", O. Pironneau, W. Rodi, I.L. Rhyming, A.M. Savill and T.V. Truong, eds. Cambridge, 318–.

Voke, P.R., Yang, Z., 1994 Numerical study of bypass transition *Phys. Fluids* 7 2256–2264